Probing the Flat-Band Limit of the Superconducting Proximity Effect in Twisted Bilayer Graphene Josephson Junctions

A. Díez-Carlón,[1,2] J. Díez-Mérida,[1,2] P. Rout,[1,2] D. Sedov,[3] P. Virtanen,[4] S. Banerjee,[3] R. P. S. Penttilä,[5] P. Altpeter,[1] K. Watanabe,[6] T. Taniguchi,[7] S.-Y. Yang,[8] K. T. Law,[9] T. T. Heikkilä,[4] P. Törmä,[5] M. S. Scheurer,[3] and D. K. Efetov[1,2,*]

[1]*Fakultät für Physik, Ludwig-Maximilians-Universität, Schellingstrasse 4, 80799 München, Germany*
[2]*Munich Center for Quantum Science and Technology (MCQST), München, Germany*
[3]*Institute for Theoretical Physics III, University of Stuttgart, 70550 Stuttgart, Germany*
[4]*Department of Physics and Nanoscience Center, University of Jyväskylä, P.O. Box 35 (YFL), FI-40014, Finland*
[5]*Department of Applied Physics, Aalto University School of Science, FI-00076 Aalto, Finland*
[6]*Research Center for Functional Materials, National Institute for Materials Science, 1-1 Namiki, Tsukuba 305-0044, Japan*
[7]*International Center for Materials Nanoarchitectonics, National Institute for Materials Science, 1-1 Namiki, Tsukuba 305-0044, Japan*
[8]*Southern University of Science and Technology, Shenzhen 518055, People's Republic of China*
[9]*Department of Physics, Hong Kong University of Science and Technology, Hong Kong, China*

(Received 5 February 2025; revised 15 May 2025; accepted 1 October 2025; published 20 November 2025)

While extensively studied in normal metals, semimetals, and semiconductors, the superconducting (SC) proximity effect remains elusive in the emerging field of flat-band systems. In this study, we probe proximity-induced superconductivity in Josephson junctions (JJs) formed between superconducting NbTiN electrodes and twisted bilayer graphene (TBG) weak links. Here, the TBG acts as a highly tunable topological flat-band system, which, due to its twist-angle-dependent bandwidth, allows us to probe the SC proximity effect at the crossover from the dispersive to the flat-band limit. Contrary to our original expectations, we find that the induced superconductivity remains strong even in the flat-band limit and gives rise to broad, dome-shaped SC regions, in the filling-dependent phase diagram. In addition, we find that, unlike in conventional JJs, the critical current I_c strongly deviates from a scaling with the normal state conductance G_N. We attribute these findings to the onset of strong electron interactions, which can give rise to an excess critical current. By also studying the dependence of I_c on the filling and twist angle across multiple samples, we further uncover the importance of quantum geometric terms as well as multiband pairing mechanisms in describing the induced superconductivity in the TBG flat bands as their bandwidth decreases. To the best of our knowledge, our results present the first detailed study of the SC proximity effect in the flat-band limit and shed new light on the mechanisms that drive the formation of SC domes in flat-band systems.

DOI: 10.1103/ccb4-tqxq

Subject Areas: Condensed Matter Physics

I. INTRODUCTION

The superconducting proximity effect at the interface of a superconductor (S) and a normal metal (N) is understood by the leaking of superconducting correlations into the normal region, through the creation of phase coherent Andreev pairs [1,2]. This process is explained by de Gennes' theory [1–5], which considers wavefunction matching across the N/S interface and typically works well for normal metals with dispersive bands, and a large Fermi velocity and Fermi surface. However, these conditions are dramatically altered in materials with a vanishing bandwidth, as found in various flat-band systems, like kagome metals [6,7], moiré materials [8], and Lieb lattices [9–11]. Recent theoretical studies have derived new formalisms to describe the superconducting (SC) proximity effect in such systems [12,13]. They show that, in atomic flat bands, the proximity effect can be strongly quenched, as their Fermi velocity vanishes and electrons localize. However, strong electronic interactions and quantum geometric terms can give rise to an enhanced conduction and

*Contact author: dmitri.efetov@lmu.de

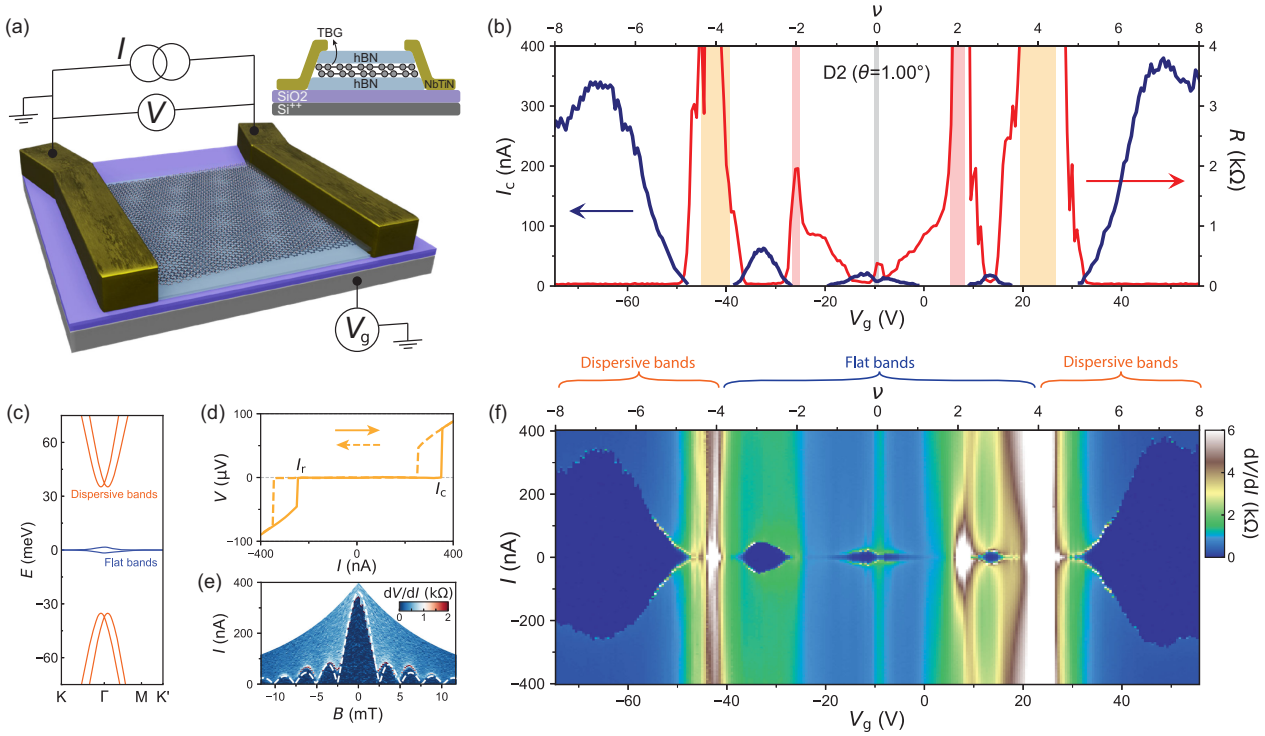

FIG. 1. Superconducting proximity effect in a TBG Josephson junction. (a) Device schematic of a TBG sheet acting as the weak link of a JJ. The voltage V across the junction is recorded as a current bias I is applied through the superconducting electrodes in a two-probe measurement. The carrier density is tuned by a gate voltage V_g to the doped Si. (b) Resistance R in red (right axis) at zero current bias, as a function of V_g (bottom) and of the corresponding moiré filling factor ν (top). Shaded vertical lines indicate the presence of the charge-neutrality point (gray), the correlated insulators at half filling of the flat bands (red), and the band insulators between the flat and dispersive bands (yellow). Regions with low resistance have a finite critical current I_c (blue, left axis), extracted from the nonlinear characteristics measured in panel (f). (c) Band structure of TBG for $\theta = 1.00°$. (d) The $I - V$ curve measured at $V_g = 50$ V. The solid and dashed lines have opposite sweep directions as indicated by the arrows. (e) Interference pattern recorded at the dispersive bands, for $V_g = 60$ V, which agrees well with a uniform single-slit junction (white dashed line). (f) Differential resistance dV/dI map, where dark blue regions represent superconducting states. Their contour along positive values of I was used for extracting I_c in panel (b). All data were obtained in device D2.

superfluidity [14–16] and, as a result, allow for a sizable SC proximity effect [12,13].

Twisted bilayer graphene (TBG) presents a highly suitable platform to test these predictions. It contains two adjacent flat bands with a bandwidth that can be tuned below $w < 10$ meV in devices with a magic twist angle of $\theta_m \sim 1.1°$, which is 3 orders of magnitude lower than in normal metals. They were previously shown to host a broad number of strongly correlated phases—such as superconductivity [17,18], correlated insulators [19,20], and nontrivial topological states [21–23]—and were argued to contain quantum geometric terms that can enhance the superconducting state [16]. In addition, the close proximity of the two flat bands in energy could, in principle, allow for the formation of more complex Andreev pairs, which could reside in both bands [24–26].

In this work, we probe the flat-band limit of the SC proximity effect by performing a detailed study of three twist-angle controlled S/TBG/S Josephson junctions (JJs) and their evolution as the bandwidth is tuned from the dispersive limit $w \sim 66$ meV ($\theta \sim 1.24°$), $w \sim 18$ meV ($\theta \sim 0.94°$) to the flat-band limit of $w < 10$ meV ($\theta \sim 1.00°$). Surprisingly, we find that, even in devices with the flattest bands, the SC proximity effect can be comparable in strength to the dispersive bands. When the Fermi energy is tuned through the flat bands, the critical current does not scale with the normal state conductance; it forms dome-shaped regions close to half filling of the bands and shows unconventional interference patterns. We discuss our findings in the context of possible contributions to the SC proximity effect through strong electron interactions, quantum geometric terms, and multiband pairing processes and provide constraints on its underlying symmetries.

II. RESULTS

A. Proximity-induced superconductivity in a TBG JJ

As depicted in Fig. 1(a), our devices consist of a van der Waals heterostructure of TBG that is encapsulated with hexagonal boron nitride dielectrics (hBN) and patterned

into a rectangular mesa of width $W \sim 1.5$ μm. The devices are capacitively coupled to a SiO_2/Si back gate that allows us to control the carrier concentration in the TBG, and they are contacted with sputtered s-wave superconducting NbTiN leads that form one-dimensional edge contacts, resulting in junctions of length $L \sim 200$ nm. It is worth noting that while several previous TBG JJ experiments used the intrinsic SC state of TBG and a gate-defined weak link [27–29], the device design presented here strongly simplifies the modeling of such JJs, as it uses a SC state with a known pairing mechanism and defines a simpler and sharper junction interface.

We first focus on device D2 with a twist angle $\theta \sim 1.00 \pm 0.01°$, slightly smaller than θ_m. All data were obtained at a temperature of 35 mK. Figure 1(b) shows two-terminal resistance R measurements as a function of gate voltage V_g as we tune through the dispersive and flat-band regions [see Fig. 1(c)], which show peaks at integer fillings of the moiré unit cell $\nu = 0$, ± 2, and ± 4. This behavior is characteristic of strongly correlated TBG devices in the range of twist angles of $\theta \sim 1.0°$–$1.2°$, where $\nu = \pm 2$ marks the occurrence of correlated insulator states [8,17–20].

Additionally, zero-resistance states at various fillings are recorded due to the SC proximity effect, as shown in Fig. 1(c), where we measure the differential resistance dV/dI as a function of dc I for the same range of V_g as Fig. 1(b). We clearly see superconducting regions with zero resistance (dark blue) that are limited by the critical current I_c [displayed in Fig. 1(b)], which exist across almost the entire density range. We observe broad dome-shaped SC regions in the dispersive bands at $|\nu| > 4$ and also in the flat bands near the charge-neutrality point (CNP) $\nu = 0$, and between fillings $\nu = \pm 2$ and $\nu = \pm 4$.

The formation of the Josephson effect is confirmed by the observation of nonlinear current-voltage characteristics, such as the one shown in Fig. 1(d) in the dispersive bands ($V_g = 50$ V, $\nu = 7.3$). The switching from the zero-resistance state to the normal state is detected as a sharp transition in voltage and presents a hysteretic behavior between the retrapping (I_r) and critical (I_c) currents, as is common for underdamped junctions or due to self-heating effects [4]. The phase coherence of the JJ is further demonstrated by the observation of Fraunhofer interference patterns when a perpendicular magnetic field B is applied to the junction, as seen in Fig. 1(e). The period of the measured oscillations $\Delta B \sim 2.5 \pm 0.2$ mT matches well with the expected periodicity $\Delta B_{\mathrm{phys}} \sim 2.3 \pm 0.1$ mT defined by the physical area of the junction around 0.33 ± 0.07 μm^2 when flux-focusing effects are included (see Supplemental Material [30] for more details).

A natural question is whether some of the zero-resistance states observed could arise from an intrinsic SC state of TBG. However, several experimental signatures argue against such an assumption. First, the observed I_c in the superconducting domes at $\nu < -2$ reaches its maximum at $\nu \sim -2.9$ and spans down to $\nu \sim -3.5$ [Fig. 1(b)], exceeding the range of filling where TBG typically shows an intrinsic SC state [8,17,18]. Moreover, while sweeping ν across this range, we see no additional switching transitions in the dV/dI curves and no abrupt changes in I_c or in the interference patterns (see Fig. S20 in the Supplemental Material [30]). In the latter, the period of the $I_c(B)$ oscillations coinciding with the junction area also suggests a lack of intrinsic superconductivity since I_c would otherwise not oscillate and instead decay monotonically with the field [28,31,32]. We then conclude that the superconductivity observed in our TBG JJs arises from the proximity effect.

B. Excess of supercurrent due to strong electron interactions in the flat bands

The maximal critical currents that we observe in the flat bands of $I_c \sim 65$ nA are only a factor of 5 lower as compared to the dispersive bands $I_c \sim 350$ nA. This finding is surprising, as we would have expected a much stronger suppression of the SC proximity effect in the flat bands as compared to the dispersive bands, given the large reduction in the bandwidth and Fermi velocity (see Supplemental Material [30]) [12,13,16,33]. Since the I_c values themselves do not allow for a direct estimate of the strength of the SC proximity effect, it is instead typically approximated with the I_cR_N product [2,4,5]. Here, R_N is the normal state resistance of the JJ, which we extract through resistance measurements at a current $I > I_c$ (see Supplemental Material [30] for more details). Figure 2(a) shows I_cR_N vs ν, where we find especially large values in the dome-shaped proximity-induced regions between fillings $\nu = \pm 2$ and $\nu = \pm 4$, which are comparable to the ones in the dispersive bands. This finding further confirms that, unlike the initial expectations, the SC proximity effect is surprisingly large in the flat bands of TBG [2,5,33].

The unexpected strength of the SC proximity effect in the flat bands is not the only peculiarity, as the filling dependence of the I_c inside the flat bands is also highly unusual. In typical JJs, Andreev pairs undergo dephasing processes, the strength of which scales with the normal state resistance R_N. It is therefore often found that I_c correlates with $G_N = R_N^{-1}$, the normal state conductance [2,4,5]. We demonstrate that this is the case in JJs with single-layer graphene or small twist-angle TBG as the weak links (see Supplemental Material [30] for comparison) [34]. The same trend is also found when looking at the dispersive bands of our device D2, as can be seen in Fig. 2(b), which shows the filling dependence of the critical current I_c vs ν and overlays it with the filling dependence of the normal state conductance G_N vs ν. In this case, the I_c generally follows the density of states by becoming stronger with increasing filling and peaking between $\nu \sim 7$ and $\nu \sim 8$ (see Supplemental Material [30], Fig. S14).

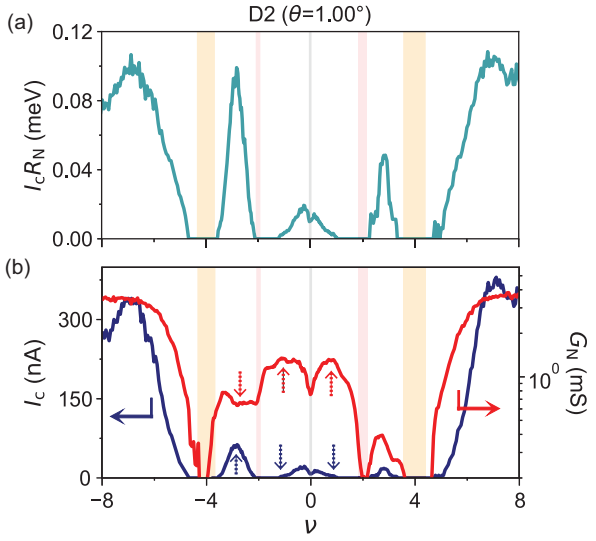

FIG. 2. Strength of the proximity effect and relation between the critical current and normal conductance. (a) Product of the critical current and normal state resistance, I_cR_N, as a function of the moiré filling factor ν. (b) Critical current I_c in blue (left axis) and normal state conductance G_N in red (right axis), both as a function of ν. Following the same color code, the dashed vertical arrows indicate whether the corresponding quantity has reached a maximum or minimum. This highlights the unusual relation between I_c and G_N found at the flat bands. All data correspond to D2. Shaded vertical lines indicate the presence of the charge-neutrality point (gray), the correlated insulators (red), and the band insulators (yellow).

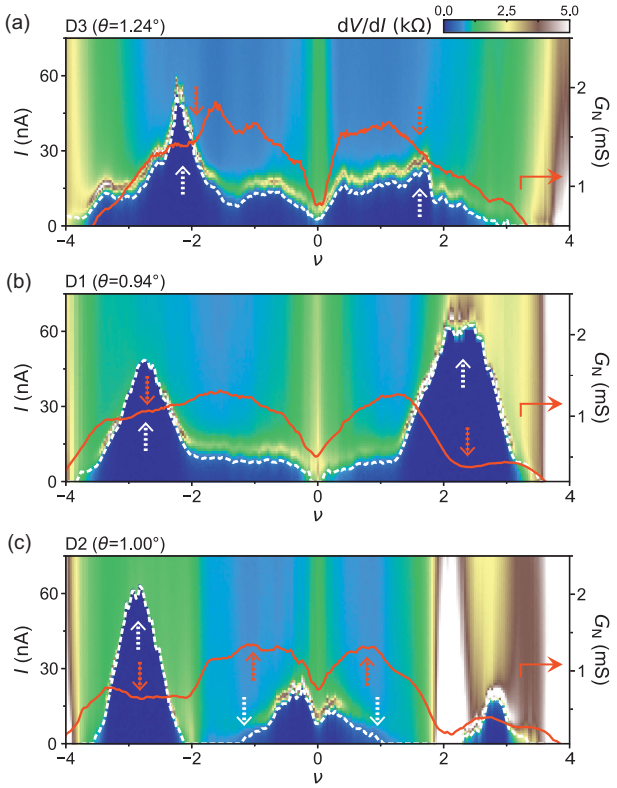

FIG. 3 Proximitized flat bands with varying bandwidth by tuning the twist angle. (a)–(c) Colormaps of measured differential resistance dV/dI as a function of dc I (left axis) and filling ν of the flat band, for devices D3, D1, and D2, respectively. The solid red line corresponds to the normal state conductance G_N (right axis). The critical current I_c of each device is extracted by following the contour of the dark blue regions in the colormaps, marked by white-dashed lines. Following the same color code, the dashed vertical arrows indicate the regions where I_c and G_N follow opposite trends, pointing to whether the corresponding quantity is an increasing or decreasing function of $|\nu|$. In D1 and D3, the observed Josephson effect holds throughout almost the entirety of the flat bands, given the absence of correlated states at integer fillings. In the case of D2 (the closest to θ_m), the superconducting phases are interrupted by insulating states at half filling.

In strong contrast, the flat bands of our devices show the exact opposite trend, as pointed out by vertical dashed arrows in Fig. 2(b) [see also Fig. 3(c)]. Here, both I_c and G_N increase when doping away from the CNP, but while I_c peaks at $|\nu| \sim 0.3$ and decreases beyond these points, finally vanishing at $|\nu| \sim 1$, G_N continues to increase until $|\nu| \sim 1$. At higher doping, with the I_c domes at $|\nu| > 2$, the same process appears: Because G_N shows smaller values than near the CNP, we expect a vanishing I_c, and yet we observe similar ($\nu > 2$) or even bigger values ($\nu < -2$). Analogous trends are also found for other devices in their flat bands [see Figs. 3(a) and 3(b)].

The deviation of the observed scaling of I_c and G_N in the flat bands could be explained by the existence of excess values of I_c in certain fillings, which could come from an extra contribution that is independent of G_N and thus of band dispersion. Such an often-neglected term, I_c^{int}, indeed exists theoretically and scales with an attractive interaction coupling between electrons, contributing to the total critical current because it boosts the Andreev pair transport through the JJ [13]. It is then an important contribution in (quasi-) flat bands, where the range of pair correlations without interactions can become short due to localization in non-interacting transport. Similarly, as in the superfluid weight, part of this increase is related to the quantum geometry and is independent of band dispersion [12,13,35,36]. As has been shown in Ref. [10] and Supplemental Material [30], I_c^{int} is independent of G_N, so the total critical current I_c does not necessarily correlate with G_N in regions where I_c^{int} dominates, as could be the case for our devices in the ranges mentioned above. We note that, for a quantitative explanation of the observed unconventional relation between I_c and G_N, future theoretical models should also derive the full contribution from the band dispersion to the I_c and compare it with I_c^{int}.

Previous experiments using gate-defined JJs in TBG [27–29] demonstrated that a finite supercurrent can flow through the flat bands and could, in principle, have accessed similar proximity-induced phenomena.

However, device limitations such as varying junction lengths with filling and the fact that the weak link cannot be studied independently from adjacent gate-tunable regions may obscure subtle deviations from the conventional Josephson effect. In addition, because the superconducting state of TBG itself may already have an unconventional pairing [17,37] as well as quantum geometry contributions to its superfluidity and coherence length [16,36,38], it becomes difficult to disentangle whether the observed features originate from the weak link or from the intrinsic properties of the flat-band superconductor. By using external s-wave superconducting leads, our experiment cleanly isolates the TBG weak link and enables systematic comparisons between flat and dispersive bands as well as across different twist angles, which we will explore next, offering a clearer study on how band structure, interactions, and quantum geometry affect the proximity-induced superconductivity.

C. Examining potential effects due to quantum geometry and multiband pairing

While we now have postulated the existence of enhanced I_c regions in the flat bands and a potential explanation related to strong electron interactions, the strong variation of I_c and the formation of dome-shaped regions, especially close to the band insulators between fillings $\nu = \pm 2$ and $\nu = \pm 4$, remain unclear. In order to obtain a better understanding of the driving forces behind these domes, we use the powerful tuning knob of TBG, the bandwidth w, which can be controlled directly by the twist angle. As we will see next, by tuning w, we can effectively tune the band dispersion and interactions.

Figure 3 compares three samples with different twist angles: D1 ($\theta \sim 0.94 \pm 0.01°$), D2 ($\theta \sim 1.00 \pm 0.01°$), and D3 ($\theta \sim 1.24 \pm 0.01°$). All three devices show a finite I_c across almost the entire flat band, with some dome-shaped regions in between half filling $\nu = \pm 2$ and the band edges $\nu = \pm 4$. It appears that as w is lowered [Figs. 4(d)–4(f)], the dome-shaped SC regions move closer to the band edges [see Figs. 3(a)–3(c)]. While I_c is suppressed in D1 and D3 close to the CNP, in D2, which has the lowest bandwidth, the region around the CNP shows enhanced I_c values.

We try to qualitatively understand the observed variation of I_c with filling and twist angle. We use the Eliashberg formalism and perturbation theory to compute the linear response function to the contact-induced pairing from an s-wave superconductor into TBG at the Fermi level E_F. Under the slowly varying field approximation, the response is captured by the superconducting pair correlation function $\phi_R = \int_{\text{u.c.}} \mathrm{da} \langle c_{\downarrow,-}(\mathrm{R}+\mathrm{a}) \cdot c_{\uparrow,+}(\mathrm{R}+\mathrm{a}) \rangle$. To model the TBG, we use the Bistritzer-MacDonald (BM) continuum model [39] and calculate the band structure, the bandwidth [see Figs. 4(d)–4(f)], and the pair correlator ϕ_R at a distance R in moiré unit cells coinciding with the center of the junctions D1-3 (see Supplemental Material [30] for more details). Here, besides the dominant-induced Andreev pair components with opposite spin $(\uparrow, \downarrow)$ and valleys $(-, +)$, a possible, small, admixed intravalley component in TBG is expected to be quickly suppressed with R. Since the correlator ϕ_R can be understood as a response function of the TBG bands to an external superconducting field, a qualitative comparison can be made with I_c.

The strength of this formalism lies in the fact that we can explicitly account for the different contributions to the correlator ϕ_R, which include the band dispersion and the quantum geometric terms. Importantly, the induced Andreev pairs do not need to reside only in a single band at the Fermi level E_F, but it can also have weight across multiple bands. The contribution from multiband pairing to ϕ_R, however, diminishes more the further these bands are from E_F and the larger their dispersion is; thus, it is expected to be significant only in the flattest bands (see Supplemental Material [30] for more details).

In order to highlight the effect of each contribution and work out the effects of the quantum geometry and multiband pairing, we separate these terms out and plot them independently in Fig. 4. Here, we consider three cases. First, we consider $\phi_R^{\text{S.B.}}$, which contains only dispersion-driven effects, by taking the atomic limit of the flat bands, where the Bloch states are completely momentum independent and the quantum geometric contribution is suppressed, and Andreev pairs that are only formed inside a single band at E_F [Fig. 4(a)]. We next consider $\phi_R^{\text{Q.G.}}$, which contains dispersion-driven effects but now departing from the atomic limit where we incorporate the overlap between Bloch states at different momenta, which is determined by the quantum metric of the bands, and Andreev pairs that are only formed inside one band at E_F [Fig. 4(b)]. Lastly, we consider $\phi_R^{\text{M.B.}}$, which contains dispersion-driven effects with a suppressed quantum geometric contribution, like in the first case, but now additional Andreev pairs formed inside other bands can interfere with the ones from the band at E_F [Fig. 4(c)].

Our calculations are shown in Figs. 4(g)–4(i) for the three different bandwidths w corresponding to the three devices shown in Fig. 3, with D3 ($w \sim 66$ meV), D1 ($w \sim 18$ meV), and D2 $w \sim 4$ meV) [BM band structures shown in Figs. 4(d)–4(f)]. Here, we find that, when the filling is varied, $\phi_R^{\text{S.B.}}$ just follows the density of states for all w (Supplemental Material [30], Fig. S13 shows this statement explicitly). It shows peaks close to half filling $\nu = \pm 2$, which rapidly decrease close to the band edges $\nu = \pm 4$ and the CNP. Although this scenario very well matches the broadest bandwidth $w \sim 66$ meV [Fig. 4(g)] with our I_c measurements [Fig. 3(a)], it dramatically fails to describe the observed features of devices D1 and D2 with lower w [see Figs. 3(b)–3(c) and 4(h)–4(i)]. For the flattest bands, $w \sim 4$ meV, the peaks in $\phi_R^{\text{S.B.}}$ strongly broaden and show an almost constant value across the entire range of ν [Fig. 4(i)], failing to produce dome-shaped regions. By now

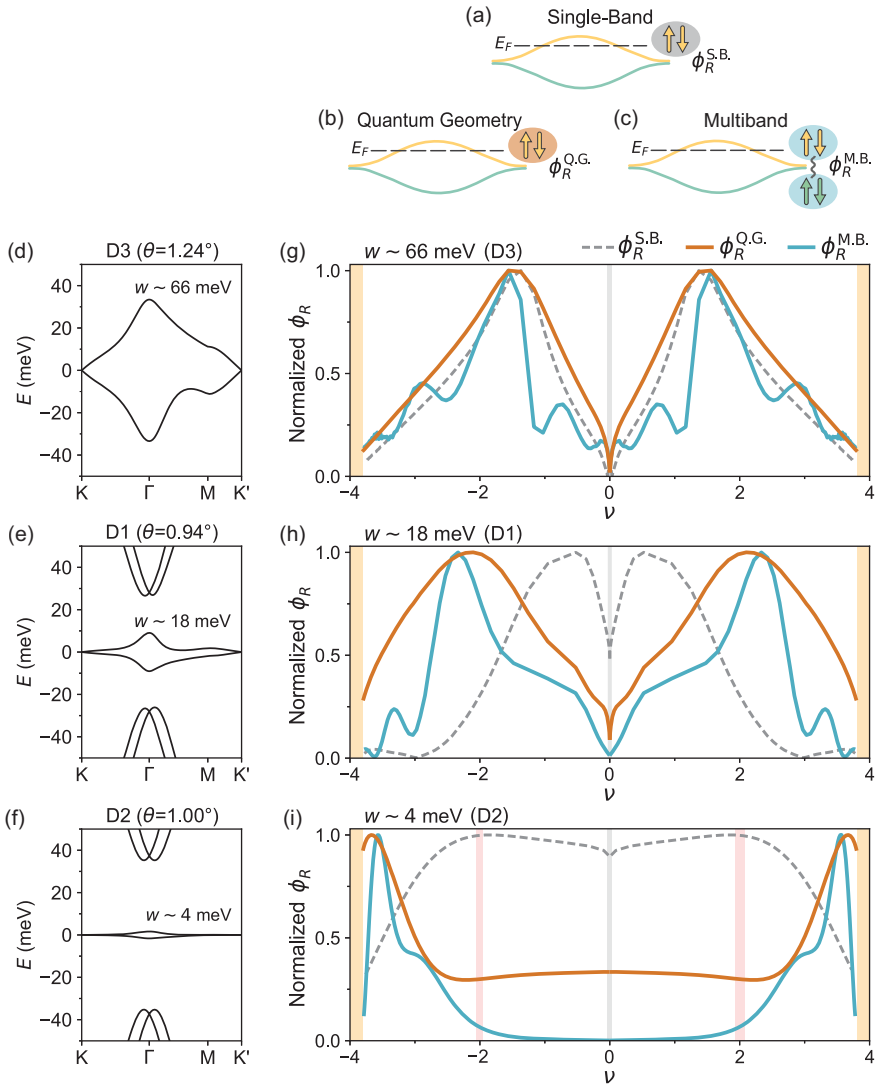

FIG. 4. Quantum geometric and multiband contributions to the induced superconductivity in the flat bands. (a)–(c) Sketches illustrating the different contributions to the induced superconductivity. The color of the spin of the electrons forming the Andreev pair indicates which band they are coming from. In panel (a), the contribution comes only from the dispersion of the same band where the Fermi level E_F lies, whereas in panel (c), the interference with more bands is also accounted for, i.e., multiband pairing. In panel (b), the quantum geometric contribution is considered along with the dispersion of the single band in panel (a). (d)–(f) Band structure of the TBG continuum model along high-symmetry points for the three different twist angles corresponding to samples D3, D1, and D2, respectively. The bandwidth w of the flat bands is also shown. (g)–(i) Computed superconducting correlator ϕ_R vs filling factor ν for the three processes illustrated in panels (a)–(c), following the same color code as the sketches of the Andreev pairs. Shaded vertical lines indicate the presence of the charge-neutrality point (gray), the correlated insulators (red), and the band insulators (yellow).

plotting $\phi_R^{\mathrm{Q.G.}}$ including quantum geometric and $\phi_R^{\mathrm{M.B.}}$ including multiband terms, we find that these are strongly altered from $\phi_R^{\mathrm{S.B.}}$ as the bandwidth is lowered, and both give rise to dome-shaped features close to the band edges, just as observed for the devices D1 with $w \sim 18$ meV and D2 with $w \sim 4$ meV. We find that, overall, the $\phi_R^{\mathrm{Q.G.}}$ term better matches the findings of the $w \sim 4$ meV case, as it allows for a finite-induced superconducting phase in the center of the band and close to the CNP, as observed in device D2. We also find that D1 with $w \sim 18$ meV is better matched with $\phi_R^{\mathrm{M.B.}}$. The moderate mismatch in D2 compared to D1 and D3 could come from the fact that only the former shows correlated states due to interactions, which are not considered in our model.

We want to stress that, to fully capture and explain the proximity effect in this correlated system, future theoretical models should further account for interactions, as our current approach does not explain the vanishing I_c due

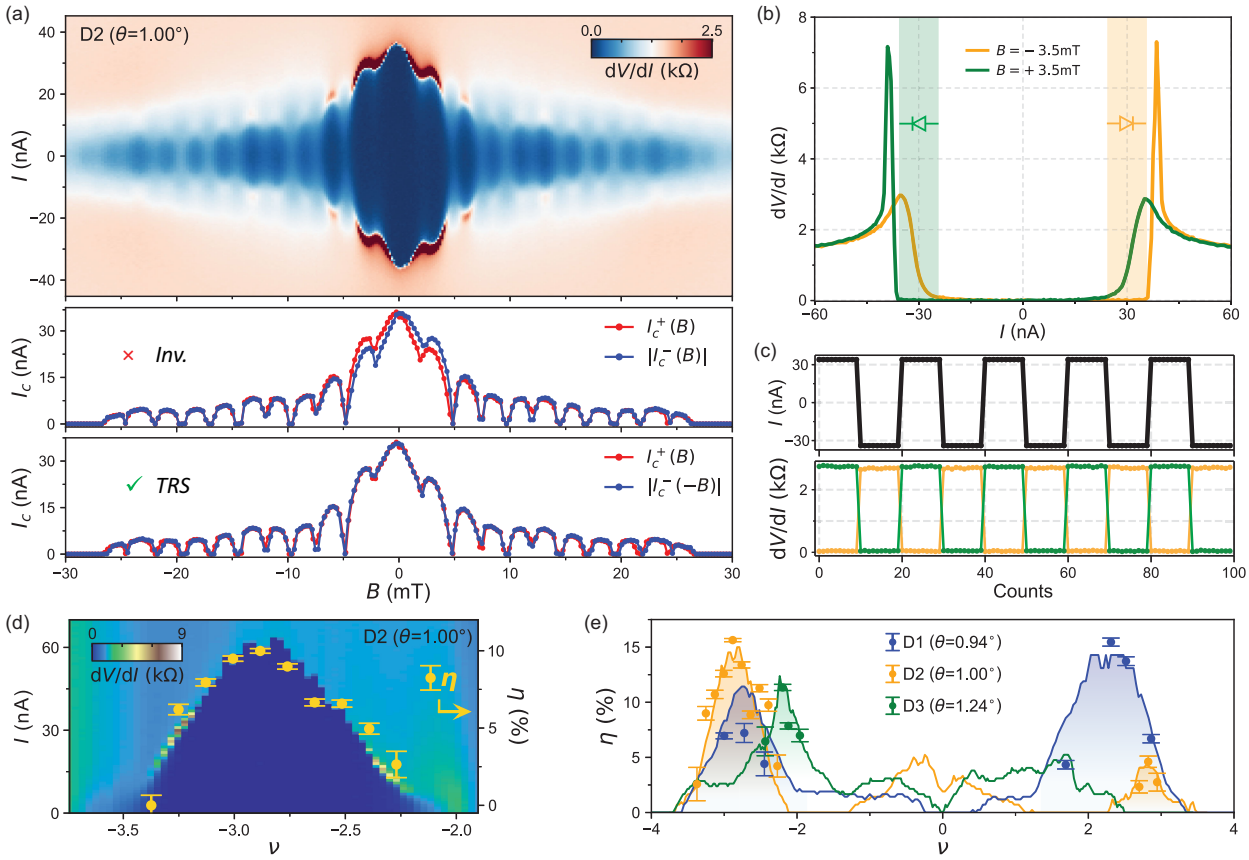

FIG. 5. Josephson diode effect and inversion symmetry breaking at the $|\nu| > 2$ domes. (a) Top panel: measured differential resistance dV/dI as a function of dc bias I and magnetic field B, at $\nu = -2.5$ for D2. The critical current of the dark-colored oscillations is extracted for positive (I_c^+) and negative (I_c^-) directions of dc. These results are represented for the same and opposite values of the magnetic field in the middle and bottom panels, respectively. (b) The dV/dI traces measured at opposite magnetic fields. Shaded regions mark the I values at which the Josephson diode is operational. The measurements are performed at $\nu = -2.9$ for D2. (c) Demonstration of the reversible JDE in panel (b), performed by switching between the superconducting and normal states when opposite currents are applied, in this case, +34 nA and −34 nA. Reversibility of the direction of the diode is achieved by applying an exactly opposite B. (d) The dV/dI colormap vs I (left axis) and ν. Represented along with the error bars is the extracted diode efficiency η (right axis) vs ν, computed at a magnetic flux $\Phi = \Phi_0/2$. All data correspond to D2. (e) Maximum value of $\eta(B)$ between $-2\Phi_0$ and $2\Phi_0$, represented with error bars and as a function of ν for all junctions near the magic angle D1-3. The line plots correspond to the I_c (in arbitrary units) from Figs. 3(d)–3(f). The shaded regions correspond to fillings where a finite asymmetry was recorded. The interference patterns where η was extracted can be found in Supplemental Material [30].

to the correlated states at integer fillings. Overall and despite the simplicity of the continuum model in describing the flat bands of TBG, the qualitative agreement with the data highlights that, when the bandwidth reaches the flat-band limit, quantum geometric and multiband processes could become important in understanding the susceptibility of TBG to develop superconducting phases [25]. It may explain the formation of dome-shaped SC regions between half filling and the band edges, which roughly coincide with the regions that typically also show intrinsic superconductivity in TBG devices at the magic angle. It is therefore interesting to consider whether similar effects as the ones that were worked out here can also explain the position of the SC domes in TBG.

D. Symmetry breaking and the Josephson diode effect

The presence of interactions in the TBG JJs at half fillings of the bands is further suggested by a consistent observation of a symmetry-broken Josephson effect, which will be the focus of the remainder of this work. We start by studying an interference pattern in D2 at $\nu = -2.5$, shown in Fig. 5(a). When recording I_c vs B in opposite directions of the dc, $I_c^+(B)$ and $I_c^-(B)$, we find that $I_c^+(B) \neq |I_c^-(B)|$, as clearly seen in the middle panel of Fig. 5(a). Such an observation indicates that inversion symmetry is broken in our JJs and is unlike the conventional symmetric patterns found near the CNP or in the dispersive bands [see Fig. 1(e) and Supplemental Material [30]]. This nonreciprocity is a hallmark of the Josephson diode effect (JDE), which

requires both inversion C_{2z} and time-reversal symmetry (TRS) breaking [40–42]. Importantly, in our devices, TRS is broken by applying an external perpendicular magnetic field to the graphene layers, which rules out Rashba spin-orbit coupling as a possible mechanism, where an in-plane magnetic field that is perpendicular to the direction of the current is needed to produce the nonreciprocity [42]. Furthermore, the TBG weak link itself does not intrinsically break TRS, as no asymmetry is recorded at zero field; i.e., we find $I_c^+(0) = |I_c^-(0)|$. This finding is further confirmed by having $I_c^+(B) = |I_c^-(-B)|$ [see bottom panel of Fig. 5(a)]; an expression that conserves this symmetry and makes the diode programmable by applying exactly opposite fields. Such programmability is illustrated in Figs. 5(b) and 5(c), where the dV/dI curves validate the aforementioned symmetry relations and the operation of the diode is demonstrated in the rectification measurements.

Notably, we find that the key features reported in Figs. 5(a)–5(c) extend across the entire filling of the dome, spanning from $\nu \sim -2$ to $\nu \sim -3.5$. This case is shown in Fig. 5(d), where the diode efficiency parameter $\eta(B) = (I_c^+(B) - |I_c^-(B)|)/(I_c^+(B) + |I_c^-(B)|)$, calculated at half the superconducting magnetic flux quantum $\Phi_0/2$, is found to correlate with the I_c of the dome. Thus, we see that the asymmetry is most pronounced at the center of the dome at $\nu = -2.9$, but it is no longer detectable at the edges of it at $\nu = -2.3$ and $\nu = -3.4$. Furthermore, our observation of inversion symmetry breaking consistently appears in the domes at the hole side of $\nu \sim -2$ for all our TBG JJs close to θ_m (D1-3) and, in some cases (D1-2), on the electron side of $\nu \sim 2$. Figure 5(e) shows that, for all devices, η correlates with the I_c of their respective domes. In this case, to compare the JDE between different devices, we have calculated the maximum value of η between $-2\Phi_0$ and $2\Phi_0$ (see Supplemental Material [30] for more details). Such an extent of the asymmetry with filling suggests a distinct phase is responsible for the JDE.

Several interacting ground states that spontaneously break the C_{2z} and spinless time-reversal symmetries of TBG have been proposed. Valley polarization was suggested to explain the abundance of orbital magnetism and broken inversion found at these bands [29,43–45], although original nematicity measurements [46,47] showed C_{3z} symmetry breaking instead. In addition, recent experiments in scanning tunneling microscopy have pointed towards the most likely candidates at such fillings having intervalley coherent or incommensurate Kekulé spiral orders [48], which do not break C_{2z}. Therefore, none of the above candidates is consistent with our findings, and a sublattice-polarized phase emerges as the only candidate that fulfills our observed symmetry relations [25,49,50], where each valley carries opposite Chern numbers $C = 1$ and $C = -1$. Since we cannot quantify the amount of strain in our samples, unlike in STM [48,51], we cannot rule out that this tuning parameter is favoring such a ground state with broken C_{2z} symmetry at these fillings. We note that this case is different from a strain-induced structural breaking of C_{2z}, which would lead to a JDE at all carrier densities.

Given the range of twist angles and fillings where the JDE is found, a natural question is whether the presence of the intrinsic superconducting phase of TBG could play a significant role. However, the observation of oscillations in I_c, with their period matching the total area of the junction [Fig. 5(a)], argues against the TBG being fully intrinsically superconducting in these devices [28,31,32]. The independence in temperature of the inductance associated with the junction is also consistent (see Supplemental Material [30]), in contrast with previous observations of asymmetric oscillations in SQUIDs with high kinetic inductance [52].

Finally, the inversion symmetry breaking resulting from geometrical factors, such as a nonuniform junction with different widths of contacts, can be ruled out in our case, given that this effect would be independent of the electron density, and yet, the JDE is only observed in the flat bands and in devices close to θ_m (see Supplemental Material [30]). Self-field effects caused by inhomogeneous current bias and screening currents [2,53] cannot be the cause of the JDE either since our small I_c results in a larger Josephson penetration length $\lambda_J = \Phi_0 t W/4\pi\mu_0 I_c \lambda_L^2 \sim 7\ \mu m$ compared to the dimensions of the junction [2,54,55]. Here, $t \sim 0.6$ nm is the thickness of TBG, and $\lambda_L \sim 400$ nm is the London penetration length of NbTiN [56]. In Fig. 5(a), it can be observed that the nodes of the I_c are lifted, which is a signature of an asymmetry in the supercurrent density profile [57,58]. Nevertheless, this node-lifting effect is, in general, not enough to provide a JDE though; in addition, higher-order terms that bring the current-phase relation into a nonsinusoidal form are needed [42,59]. Such higher harmonics or anomalous phases could be a result of a symmetry-broken state as discussed above [60,61], or they can be a result of topological edge states [62,63]. The latter could also be related to our samples, given that the supercurrent is mostly carried by the edges where the JDE is observed (see Supplemental Material [30]). Testing these possible mechanisms would require phase-sensitive measurements, which we leave for future works.

III. CONCLUSIONS

To summarize, we have explored the versatility of TBG to support an extrinsic s-wave-mediated Josephson effect in its entire electronic band structure. The dispersive bands, as well as other devices away from the magic angle, served as a reference to compare the proximity effect with the flat-band limit and test its predictions. Our observation of an unconventional scaling between the critical current and the normal state conductance in the flat bands suggests an extra term in the I_c, potentially due to an attractive interaction coupling between electrons. Furthermore, our study of the formation of dome-shaped SC regions as a function of

filling and twist angle hints at quantum geometric and multiband pairing contributions being increasingly important in their enhancement as the bandwidth of the flat bands narrows. Overall, to the best of our knowledge, our work constitutes the first experimental effort to characterize in detail the superconducting proximity effect in a flat-band system. Future works should focus on fully incorporating strong interactions in the mechanism of induced superconductivity in TBG, in order to explain symmetry-broken effects such as the Josephson diode effect.

ACKNOWLEDGMENTS

We thank Srijit Goswami for help in sample fabrication. D. K. E. acknowledges funding from the European Research Council (ERC) under the European Union's Horizon 2020 research and innovation program (Grant Agreement No. 852927), the German Research Foundation (DFG) under the priority program SPP2244 (Project No. 535146365), the EU EIC Pathfinder Grant "FLATS" (Grant Agreement No. 101099139), and the Keele, Kavli, Tschira, and Wells Foundations as part of the SuperC Collaboration. K. W. and T. T. acknowledge support from the Elemental Strategy Initiative conducted by the MEXT, Japan (Grant No. JPMXP0112101001) and JSPS KAKENHI (Grants No. 19H05790, No. 20H00354, and No. 21H05233). R. P. S. P. acknowledges financial support from the Fortum and Neste Foundation. This work was supported by the Research Council of Finland under Projects No. 339313 and No. 354735, by European Union's HORIZON-RIA programme 331 (Grant Agreement No. 101135240 JOGATE), by the Jane and Aatos Erkko Foundation, the Keele Foundation, and the Magnus Ehrnrooth Foundation as part of the SuperC Collaboration, and by a grant from the Simons Foundation (SFI-MPS-NFS-00006741-12, P. T.) in the Simons Collaboration on New Frontiers in Superconductivity. D. S., S. B., and M. S. S. acknowledge funding by the European Union (ERC-2021-STG, Project No. 101040651—SuperCorr).

A. D. C., S. Y. Y., and D. K. E. conceived and designed the experiments; A. D. C. and P.R. fabricated the devices; A.D.C. performed the measurements and analyzed the data; D. S., P. V., S. B., R. P. S. P., T. T. H., P. T., and M. S. S. performed the theoretical analysis; T. T. and K. W. provided materials; D. K. E. supported the experiments; A. D. C. and D. K. E. wrote the paper with input from J. D. M., D. S., P. V., T. T. H., P. T., and M. S. S.

The authors declare no competing interests.

Views and opinions expressed are those of the authors only and do not necessarily reflect those of the European Union or the European Research Council Executive Agency. Neither the European Union nor the granting authority can be held responsible

DATA AVAILABILITY

The data that support the findings of this study are available from the corresponding author upon reasonable request.

[1] P. G. De Gennes, *Boundary effects in superconductors*, Rev. Mod. Phys. **36**, 225 (1964).
[2] K. K. Likharev, *Superconducting weak links*, Rev. Mod. Phys. **51**, 101 (1979).
[3] T. M. Klapwijk, *Proximity effect from an Andreev perspective*, J. Supercond. **17**, 593 (2004).
[4] M. Tinkham, *Introduction to Superconductivity* (Dover, Mineola, 1996).
[5] A. A. Golubov, M. Yu. Kupriyanov, and E. Il'ichev, *The current-phase relation in Josephson junctions*, Rev. Mod. Phys. **76**, 411 (2004).
[6] Z. Li *et al.*, *Realization of flat band with possible nontrivial topology in electronic kagome lattice*, Sci. Adv. **4**, eaau4511 (2018).
[7] M. Kang *et al.*, *Dirac fermions and flat bands in the ideal kagome metal* FeSn, Nat. Mater. **19**, 163 (2020).
[8] L. Balents, C. R. Dean, D. K. Efetov, and A. F. Young, *Superconductivity and strong correlations in moiré flat bands*, Nat. Phys. **16**, 725 (2020).
[9] S. Mukherjee, A. Spracklen, D. Choudhury, N. Goldman, P. Öhberg, E. Andersson, and R. R. Thomson, *Observation of a localized flat-band state in a photonic Lieb lattice*, Phys. Rev. Lett. **114**, 245504 (2015).
[10] A. Julku, S. Peotta, T. I. Vanhala, D.-H. Kim, and P. Törmä, *Geometric origin of superfluidity in the Lieb-lattice flat band*, Phys. Rev. Lett. **117**, 045303 (2016).
[11] S. Ahmadkhani and M. V. Hosseini, *Superconducting proximity effect in flat band systems*, J. Phys. Condens. Matter **32**, 315504 (2020).
[12] Z. C. F. Li, Y. Deng, S. A. Chen, D. K. Efetov, and K. T. Law, *Flat band Josephson junctions with quantum metric*, Phys. Rev. Res. **7**, 023273 (2025).
[13] P. Virtanen, R. P. S. Penttilä, P. Törmä, A. Díez-Carlón, D. K. Efetov, and T. T. Heikkilä, *Superconducting junctions with flat bands*, Phys. Rev. B **112**, L100502 (2025).
[14] S. Peotta and P. Törmä, *Superfluidity in topologically nontrivial flat bands*, Nat. Commun. **6**, 1 (2015).
[15] P. Törmä, S. Peotta, and B. A. Bernevig, *Superconductivity, superfluidity and quantum geometry in twisted multilayer systems*, Nat. Rev. Phys. **4**, 528 (2022).
[16] H. Tian *et al.*, *Evidence for Dirac flat band superconductivity enabled by quantum geometry*, Nature (London) **614**, 440 (2023).
[17] Y. Cao, V. Fatemi, S. Fang, K. Watanabe, T. Taniguchi, E. Kaxiras, and P. Jarillo-Herrero, *Unconventional superconductivity in magic-angle graphene superlattices*, Nature (London) **556**, 43 (2018).

[18] X. Lu *et al.*, *Superconductors, orbital magnets and correlated states in magic-angle bilayer graphene*, Nature (London) **574**, 653 (2019).

[19] Y. Cao *et al.*, *Correlated insulator behaviour at half-filling in magic-angle graphene superlattices*, Nature (London) **556**, 80 (2018).

[20] M. Yankowitz, S. Chen, H. Polshyn, Y. Zhang, K. Watanabe, T. Taniguchi, D. Graf, A. F. Young, and C. R. Dean, *Tuning superconductivity in twisted bilayer graphene*, Science **363**, 1059 (2019).

[21] M. Serlin, C. L. Tschirhart, H. Polshyn, Y. Zhang, J. Zhu, K. Watanabe, T. Taniguchi, L. Balents, and A. F. Young, *Intrinsic quantized anomalous Hall effect in a moiré heterostructure*, Science **367**, 900 (2020).

[22] K. P. Nuckolls, M. Oh, D. Wong, B. Lian, K. Watanabe, T. Taniguchi, B. A. Bernevig, and A. Yazdani, *Strongly correlated Chern insulators in magic-angle twisted bilayer graphene*, Nature (London) **588**, 610 (2020).

[23] I. Das, X. Lu, J. Herzog-Arbeitman, Z.-D. Song, K. Watanabe, T. Taniguchi, B. A. Bernevig, and D. K. Efetov, *Symmetry-broken Chern insulators and Rashba-like Landau-level crossings in magic-angle bilayer graphene*, Nat. Phys. **17**, 710 (2021).

[24] A. Bussmann-Holder, H. Keller, A. Simon, and A. Bianconi, *Multi-band superconductivity and the steep band/flat band scenario*, Condens. Matter **4**, 91 (2019).

[25] M. Christos, S. Sachdev, and M. S. Scheurer, *Nodal band-off-diagonal superconductivity in twisted graphene superlattices*, Nat. Commun. **14**, 1 (2023).

[26] R. Khasanov, B.-B. Ruan, Y.-Q. Shi, G.-F. Chen, H. Luetkens, Z.-A. Ren, and Z. Guguchia, *Tuning of the flat band and its impact on superconductivity in Mo5Si3–xPx*, Nat. Commun. **15**, 2197 (2024).

[27] F. K. de Vries, E. Portolés, G. Zheng, T. Taniguchi, K. Watanabe, T. Ihn, K. Ensslin, and P. Rickhaus, *Gate-defined Josephson junctions in magic-angle twisted bilayer graphene*, Nat. Nanotechnol. **16**, 760 (2021).

[28] D. Rodan-Legrain, Y. Cao, J. M. Park, S. C. de la Barrera, M. T. Randeria, K. Watanabe, T. Taniguchi, and P. Jarillo-Herrero, *Highly tunable junctions and non-local Josephson effect in magic-angle graphene tunnelling devices*, Nat. Nanotechnol. **16**, 769 (2021).

[29] J. Díez-Mérida *et al.*, *Symmetry-broken Josephson junctions and superconducting diodes in magic-angle twisted bilayer graphene*, Nat. Commun. **14**, 1 (2023).

[30] See Supplemental Material at http://link.aps.org/supplemental/10.1103/ccb4-tqxq for [brief description].

[31] R. Jha, M. Endres, K. Watanabe, T. Taniguchi, M. Banerjee, C. Schönenberger, and P. Karnatak, *Large tunable kinetic inductance in a twisted graphene superconductor*, Phys. Rev. Lett. **134**, 216001 (2025).

[32] M. R. Sinko, S. C. De La Barrera, O. Lanes, K. Watanabe, T. Taniguchi, S. Tan, D. Pekker, M. Hatridge, and B. M. Hunt, *Superconducting contact and quantum interference between two-dimensional van der Waals and three-dimensional conventional superconductors*, Phys. Rev. Mater. **5**, 014001 (2021).

[33] P. Dubos, H. Courtois, B. Pannetier, F. K. Wilhelm, A. D. Zaikin, and G. Schön, *Josephson critical current in a long mesoscopic $S-N-S$ junction*, Phys. Rev. B **63**, 064502 (2001).

[34] H. B. Heersche, P. Jarillo-Herrero, J. B. Oostinga, L. M. K. Vandersypen, and A. F. Morpurgo, *Bipolar supercurrent in graphene*, Nature (London) **446**, 56 (2007).

[35] S. A. Chen and K. T. Law, *Ginzburg-Landau theory of flat-band superconductors with quantum metric*, Phys. Rev. Lett. **132**, 026002 (2024).

[36] J.-X. Hu, S. A. Chen, and K. T. Law, *Anomalous coherence length in superconductors with quantum metric*, Commun. Phys. **8**, 20 (2025).

[37] M. Oh, K. P. Nuckolls, D. Wong, R. L. Lee, X. Liu, K. Watanabe, T. Taniguchi, and A. Yazdani, *Evidence for unconventional superconductivity in twisted bilayer graphene*, Nature (London) **600**, 240 (2021).

[38] M. Tanaka *et al.*, *Superfluid stiffness of magic-angle twisted bilayer graphene*, Nature (London) **638**, 99 (2025).

[39] R. Bistritzer and A. H. MacDonald, *Moiré bands in twisted double-layer graphene*, Proc. Natl. Acad. Sci. U.S.A. **108**, 12233 (2011).

[40] J. Hu, C. Wu, and X. Dai, *Proposed design of a Josephson diode*, Phys. Rev. Lett. **99**, 067004 (2007).

[41] F. Ando, Y. Miyasaka, T. Li, J. Ishizuka, T. Arakawa, Y. Shiota, T. Moriyama, Y. Yanase, and T. Ono, *Observation of superconducting diode effect*, Nature (London) **584**, 373 (2020).

[42] M. Nadeem, M. S. Fuhrer, and X. Wang, *The superconducting diode effect*, Nat. Rev. Phys. **5**, 558 (2023).

[43] J.-X. Lin, P. Siriviboon, H. D. Scammell, S. Liu, D. Rhodes, K. Watanabe, T. Taniguchi, J. Hone, M. S. Scheurer, and J. I. A. Li, *Zero-field superconducting diode effect in small-twist-angle trilayer graphene*, Nat. Phys. **18**, 1221 (2022).

[44] C.-C. Tseng, X. Ma, Z. Liu, K. Watanabe, T. Taniguchi, J.-H. Chu, and M. Yankowitz, *Anomalous Hall effect at half filling in twisted bilayer graphene*, Nat. Phys. **18**, 1038 (2022).

[45] J.-X. Hu, Z.-T. Sun, Y.-M. Xie, and K. T. Law, *Josephson diode effect induced by valley polarization in twisted bilayer graphene*, Phys. Rev. Lett. **130**, 266003 (2023).

[46] Y. Jiang, X. Lai, K. Watanabe, T. Taniguchi, K. Haule, J. Mao, and E. Y. Andrei, *Charge order and broken rotational symmetry in magic-angle twisted bilayer graphene*, Nature (London) **573**, 91 (2019).

[47] Y. Cao, D. Rodan-Legrain, J. M. Park, N. F. Q. Yuan, K. Watanabe, T. Taniguchi, R. M. Fernandes, L. Fu, and P. Jarillo-Herrero, *Nematicity and competing orders in superconducting magic-angle graphene*, Science **372**, 264 (2021).

[48] K. P. Nuckolls *et al.*, *Quantum textures of the many-body wavefunctions in magic-angle graphene*, Nature (London) **620**, 525 (2023).

[49] N. Bultinck, E. Khalaf, S. Liu, S. Chatterjee, A. Vishwanath, and M. P. Zaletel, *Ground state and hidden symmetry of magic-angle graphene at even integer filling*, Phys. Rev. X **10**, 031034 (2020).

[50] M. Christos, S. Sachdev, and M. S. Scheurer, *Correlated insulators, semimetals, and superconductivity in twisted trilayer graphene*, Phys. Rev. X **12**, 021018 (2022).

[51] F. Mesple, A. Missaoui, T. Cea, L. Huder, F. Guinea, G. Trambly de Laissardière, C. Chapelier, and V. T. Renard, *Heterostrain determines flat bands in magic-angle twisted graphene layers*, Phys. Rev. Lett. **127**, 126405 (2021).

[52] E. Portolés, S. Iwakiri, G. Zheng, P. Rickhaus, T. Taniguchi, K. Watanabe, T. Ihn, K. Ensslin, and F. K. de Vries, *A tunable monolithic SQUID in twisted bilayer graphene*, Nat. Nanotechnol. **17**, 1159 (2022).

[53] T. Golod and V. M. Krasnov, *Demonstration of a superconducting diode-with-memory, operational at zero magnetic field with switchable nonreciprocity*, Nat. Commun. **13**, 1 (2022).

[54] F. Tafuri, *Fundamentals and Frontiers of the Josephson Effect* (Springer International Publishing, New York, 2019), Vol. 286.

[55] J. R. Clem, *Josephson junctions in thin and narrow rectangular superconducting strips*, Phys. Rev. B **81**, 144515 (2010).

[56] J. G. Kroll *et al.*, *Magnetic-field-resilient superconducting coplanar-waveguide resonators for hybrid circuit quantum electrodynamics experiments*, Phys. Rev. Appl. **11**, 064053 (2019).

[57] R. C. Dynes and T. A. Fulton, *Supercurrent density distribution in Josephson junctions*, Phys. Rev. B **3**, 3015 (1971).

[58] S. Hart, H. Ren, T. Wagner, P. Leubner, M. Mühlbauer, C. Brüne, H. Buhmann, L. W. Molenkamp, and A. Yacoby, *Induced superconductivity in the quantum spin Hall edge*, Nat. Phys. **10**, 638 (2014).

[59] S. Chen *et al.*, *Current induced hidden states in Josephson junctions*, Nat. Commun. **15**, 8059 (2024).

[60] M. Alvarado, P. Burset, and A. L. Yeyati, *Intrinsic nonmagnetic ϕ_0 Josephson junctions in twisted bilayer graphene*, Phys. Rev. Res. **5**, L032033 (2023).

[61] H. Sainz-Cruz, P. A. Pantaleón, V. T. Phong, A. Jimeno-Pozo, and F. Guinea, *Junctions and superconducting symmetry in twisted bilayer graphene*, Phys. Rev. Lett. **131**, 016003 (2023).

[62] C.-Z. Chen, J. J. He, M. N. Ali, G.-H. Lee, K. C. Fong, and K. T. Law, *Asymmetric Josephson effect in inversion symmetry breaking topological materials*, Phys. Rev. B **98**, 075430 (2018).

[63] M. Endres, A. Kononov, H. S. Arachchige, J. Yan, D. Mandrus, K. Watanabe, T. Taniguchi, and C. Schönenberger, *Current–phase relation of a WTe_2 Josephson junction*, Nano Lett. **23**, 4654 (2023).